Supplementary material:

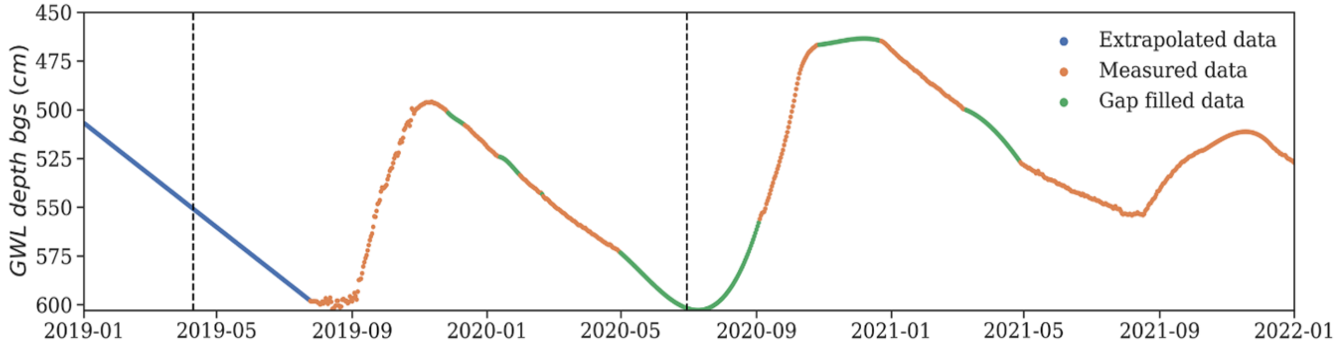

Figure S1: Groundwater dynamic (GWL) and depth below the ground surface (bgs). Source: Diongue et al., (2023).

Table S1: List of parameters used in ORCHIDEE for millet and *Faidherbia albida*

Process involved and parameters descriptions	Parameters notations	Values Tree	Values Crop	References Tree	References Crop
Soil properties					
Clay fraction (%)	clay_fraction	4		Diongue et al., (2022) Roupsard et al., (2020)	
Silt fraction (%)	silt_fraction	12.45			
Sand fraction (%)	sand_fraction	87.15			
Bulk density (kg m^{-3})	bulk_default	1710			
Soil pH (-)	soil_ph	5.75			
Flag to prescribe soil type (-)	impose_soilt	TRUE		This study	
Soil depth					
Maximum depth of soil moisture (m)	depth_max_h	7		Siegwart et al., (2023)	
Maximum depth of the root profile (m)	max_root_depth	7	2		
Maximum active layer thickness (m)	maxaltmax	15		This study	
Start depth of constant layer thickness (m)	depth_cstthick	0.123		This study	
Soil water content forcing					
Depth at which the hydrology layers will be refined towards the bottom (-)	refinebottom	TRUE		This study	
Activate nudging of soil moisture (-)	ok_nudge_mc	TRUE			
Prescribed water depth (m)	zwt_force	4	10		
Soil hydraulic					
Retention curve coefficient (n) (-)	nvan_imp	1.89		Diongue et al., (2022)	
Retention curve coefficient (α) (m m^{-1})	avan_imp	0.00075			
Residual water content (m^3 m^{-3})	mcr_imp	0.065			
Saturated water content (m^3 m^{-3})	mcs_imp	0.43			
Hydraulic conductivity saturation (mm d^{-1})	ks_imp	1060			
Water content at field capacity (m^3 m^{-3})	mcfc_imp	0.11			
Water content at wilting point (m^3 m^{-3})	mcw_imp	0.0884			
Activation flag Van Genuchten model (-)	is_vg	TRUE		This study	
Soil conductivity decay factor (-)	kfact_decay_rate	0		This study	
Development and phenological stages					
Minimum time since season (days)	min_growthinit_time	315	340	This study	
Minimum time elapsed	hum_min_time	360	350		
Leaf longevity (days)	longevity_leaf	170	200		
Length of leaf senescence (days)	leaffall	30	20		
Timescales for phenology process (days)	tau_hum_month	25			
Monthly temperature threshold above which tendency doesn't matter (°C)	t_always_add	11			

Table S1. (continued)

Process involved and parameters descriptions	Parameters notations	Values		References	
		Tree	Crop	Tree	Crop
Leaf area index					
Minimum leaf-to-sapwood area ratio (-)	k_latosa_min	5000	6000	This study	
Maximum leaf-to-sapwood area ratio (-)	k_latosa_max	6000	7000		
Allometric					
Wood density (gC m^{-3})	pipe_density	280250	-	Wickens, (1995)	-
Form factor for cylinder volume reduction (-)	tree_ff	0.6	-	This study	-
Height factor (-)	pipe_tune3	0.25	-	This study	-
Height factor (-)	pipe_tune2	15	-	This study	-
Minimum diameter of a new stand (m)	dia_init_min	0.01	-	This study	-
Maximum diameter of a new stand (m)	dia_init_max	0.02	-	This study	-
Height of a new vegetation (m)	height_init	-	0.1	-	This study
Conversion factor from LAI to height (-)	lai_to_height	-	0.6	-	This study
Total of plants (ind ha-1)	nmaxplants	-	9000	-	Sow et al., (2024)
Canopy cover (-)	canopy_cover	-	0.81	-	Sow et al., (2024)
Photosynthesis and carbon allocation					
Lower bound factor for nitrogen use efficiency (-)	sugar_load_min	0.9		This study	This study
Light absorption efficiency (mol e− (mol photon) $^{-1}$)	alpha_LL	1	0.5	This study	This study
Intercept of Jmax25/Vcmax25 (µmol e- (µmol CO_2)$^{-1}$)	arJV	1.95	2	This study	This study
Slope of Jmax25/Vcmax25 (µmol e- (µmol CO_2)$^{-1}$)	brJV	0	0	This study	This study
Nitrogen use efficiency (µmol [CO_2] s^{-1}) (gN[leaf])$^{-1}$)	nue_opt	120	60	This study	Kattge et al., (2009)
Deactivation energy for Vcmax (kJ mol^{-1})	D_Vcmax	202.9	192	Harley et al., (1992)	Massad et al., (2007)
Deactivation energy for Jmax (kJ mol^{-1})	D_Jmax	201	192	Harley et al., (1992)	Massad et al., (2007)
Entropy term function for Vcmax (J K^{-1} mol^{-1})	aSV	650	641.6	Harley et al., (1992)	Default
Convexity term for electron transport (-)	theta	0.9	0.7	Thornley, (2002)	Von Caemmerer, (2000)
Activation energy for Vcmax (kJ mol^{-1})	E_Vcmax	65.33	67.30	Chen et al., (2008)	This study
Activation energy for Jmax (kJ mol^{-1})	E_Jmax	79.5	77.9	Chen et al., (2008)	Massad et al., (2007)
Entropy term function for Jmax (J K^{-1} mol^{-1})	aSJ	650	630	Chen et al., (2008)	Massad et al., (2007)
Michaelis–Menten constant for O_2 at 25°C (mbar)	kmO25	414.5	450	Chen et al., (2008)	Von Caemmerer, (2000)
Michaelis–Menten constant for CO_2 at 25°C (µbar)	kmC25	270	650	Bernacchi et al., (2002)	Von Caemmerer, (2000)
Rubisco specificity factor (bar bar^{-1})	Sco25	2321	2590	Harley et al., (1992)	Von Caemmerer, (2000)
Evapotranspiration and vegetation structure					
Structural resistance (s m^{-1})	rstruct_const	2	0.002		
Canopy resistance parameter (-)	rveg_pft	0.01	0.7	This study	
Structural resistance (s m^{-1})	rstruct_const	2	0.002		

Table S2: Plant functional types (PFT) and their fraction used in this study.

Plant functional type	0 trees	7 trees	13 trees	26 trees
Bare soil	0.1	0.1	0.1	0.1
Tropical deciduous summer-green trees	0	0.075	0.15	0.3
C4 crop	0.9	0.825	0.75	0.6

Text S1: Vegetation water stress calculation

In the ORCHIDEE model, vegetation's water stress is used to trigger phenology and influence vegetation growth. Vegetation's water stress for *Faidherbia albida* is calculated across the entire soil column, incorporating the functional root profile as a weighting factor. The root profile, representing the fraction of root mass distributed across each soil layer based on the availability of water, is defined as:

$$Rf(i) = \begin{cases} 0, & \text{if } i < i_{4m} \\ 0, & \text{if } i \geq i_{4m} \text{ and } \sum_{i=i_{4m}}^{n} \max\left(0, W_i - W_{p,i}\right) \leq 0 \\ \frac{\max\left(0, W_i - W_{p,i}\right)}{\sum_{i=i_{4m}}^{n} \max\left(0, W_i - W_{p,i}\right)}, & \text{if } i \geq i_{4m} \text{ and } \sum_{i=i_{4m}}^{n} \max\left(0, W_i - W_{p,i}\right) > 0 \end{cases} \quad (1)$$

where i is the index for each soil layer, i_{4m} represents the index of the soil layer at 4 m, Rf represents the root profile at position i (unitless) and ranges between 0 and 1, n is the total of soil layers, W_i represents the soil moisture at position i (kg m^{-2}) and $W_{p,i}$ represents the wilting point moisture at position i (kg m^{-2}).

Then, vegetation water stress (Wstress) for *Faidherbia albida* is then given by:

$$W_{\text{stress}} = \sum_{i=1}^{n} \min\left(1, \max\left(0, \frac{\left(W_i - W_{p,i}\right)}{\left(W_{f,i} - W_{p,i}\right)}\right)\right) \times Rf(i) \quad (2)$$

where i is the index for each soil layer, n is the total of soil layers, W_i represents the soil moisture at position i (kg m^{-2}), $W_{p,i}$ represents the wilting point moisture at position i (kg m^{-2}) and $W_{f,i}$ is the soil moisture of each layer at field capacity (kg m^{-2}).

Text S2: In-situ climate data description

Mean annual air temperature was 27.78°C, with extremes' daily means ranging from a minimum of 20.27°C in 2021 to a maximum of 34.91°C in 2023. The data revealed interannual variability in precipitation, where 2022 was the wettest year (821.62 mm of cumulative annual rain) while 2018 and 2021 were drier (454.42 mm and 482.37 mm of cumulative annual rain). The years 2019, 2020, and 2023 experienced moderate rainfall, with totals of 513 mm, 599 mm, and 537 mm of cumulative annual rain, respectively. Relative humidity fluctuated between extremes' daily of 6.09% and 94.60%, observed in 2018 and 2022 respectively, with a yearly mean of 53.90%. Daily atmospheric pressure varied from 1002.03 hPa in 2022 to 1012.96 hPa in 2018, with a yearly mean of 1006.96 hPa. Daily wind speeds ranged from 1.20 m s^{-1} to 7.27 m s^{-1} both recorded in 2023, with an annual mean wind speed of 3.23 m s^{-1}. Shortwave radiation experienced a daily minimum of 67.80 W m^{-2} in 2020 and a daily maximum of 383.20 W m^{-2} in 2022, with a yearly mean of 283 W m^{-2}. Long-wave radiation measurements indicated a daily minimum of 323.40 W m^{-2} in 2023 and a daily maximum of 350.88 W m^{-2} in 2021, with a yearly average of 337.34 W m^{-2}.

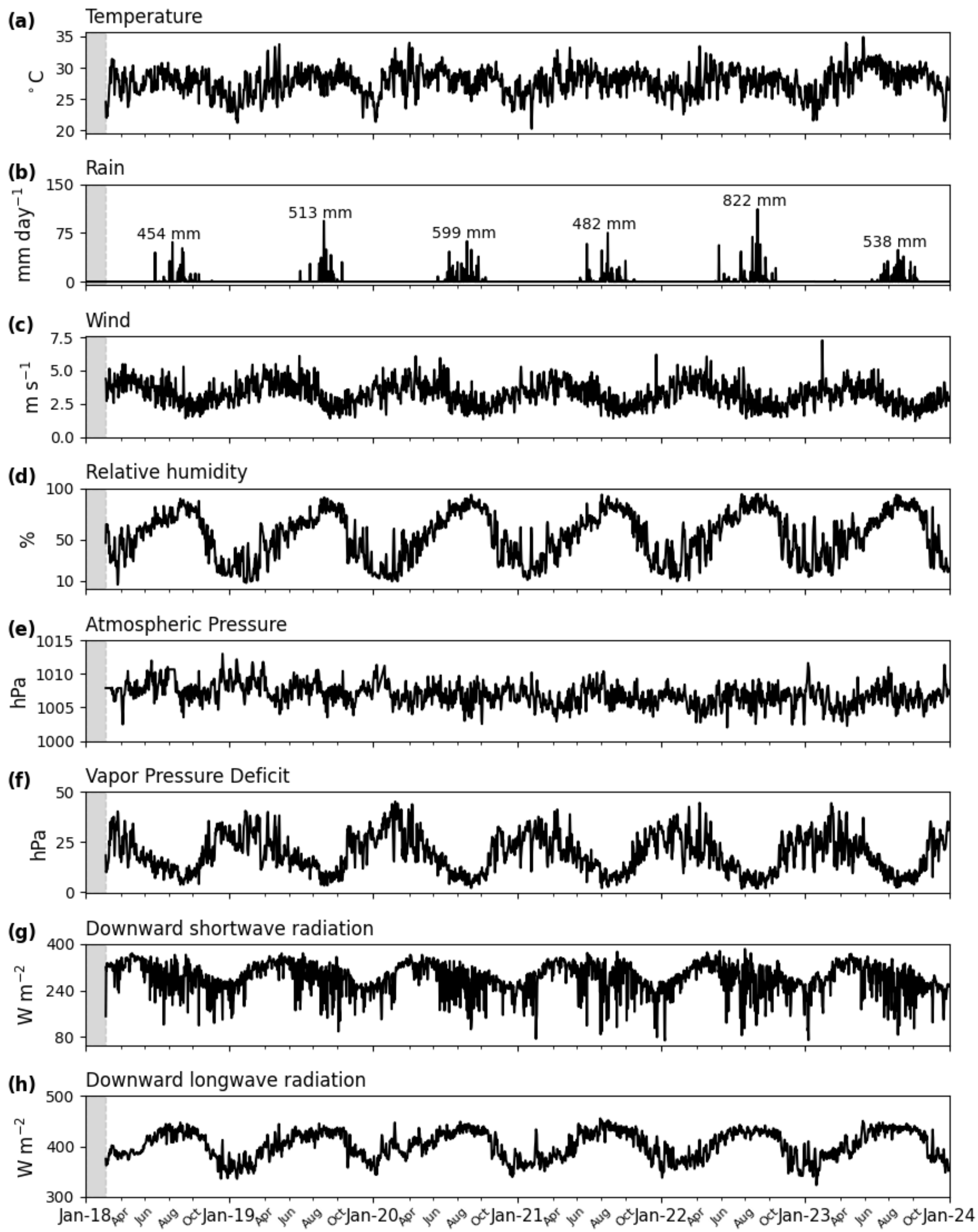

Figure S2: Daily time series of each in situ climate variable: (a) temperature, (b) rainfall and its cumulative annual rain, (c) wind, (d) relative humidity, (e) atmospheric pressure, (f) vapor pressure deficit, (g) downward longwave radiation, (h) downward shortwave radiation. The gray band represents the period of missing data.

140

Text S3: Average cycles of rainfall and soil water content in the capillary fringe

The average yearly cycles were calculated from total annual rainfall throughout five years, from 2018 to 2022 for precipitation, and from 2019 to 2021 for soil water content in the capillary fringe of the groundwater table (SWCC) with values as detailed below. For the average precipitation cycle, the average annual sum of precipitation over the analysis period was 574 mm. The maximum recorded rainfall in a single day was 81 mm. The average precipitation, calculated over the five years, was 1.59 ± 7.26 mm per day for 52 rainy days per year. The first rainy day, second rainy day, second-to-last rainy day, and last rainy day were recorded as 18 May, 20 June, 22 October, and 17 November, respectively. The second-to-last and the end of the rainy season were recorded as 22 October and 17 November, respectively. In addition, a daily average of temperature and relative humidity over the 5 years was used to constitute the average climate values for the various sensitivity analyses.

For the averaged SWCC cycle, the annual average SWCC measured by TDR probe at 4.8 m deep in the capillary fringe of the groundwater was 0.21 $m^3 m^{-3}$. The lowest recorded SWCC value was 0.15 $m^3 m^{-3}$, indicating a drier period, while the highest value reached 0.31 $m^3 m^{-3}$, indicating a wetter period. On the 1st of January, the annual average SWCC was 0.26 $m^3 m^{-3}$. The decline in the groundwater was observed until 8 July, corresponding to the lowest SWCC value. Then it remained constant until 10 September, when it began to rise again until the 24th of October. The total duration of the rise in the groundwater was 31 days, with the maximum level reached on the 24th of October. Noteworthy, the recharge occurred by the very end of the wet season, as a fast but much-delayed process compared to rainfall and this recharge also coincided with the budburst of Faidherbia occurring by mid-October, according to Roupsard et al., (2022).

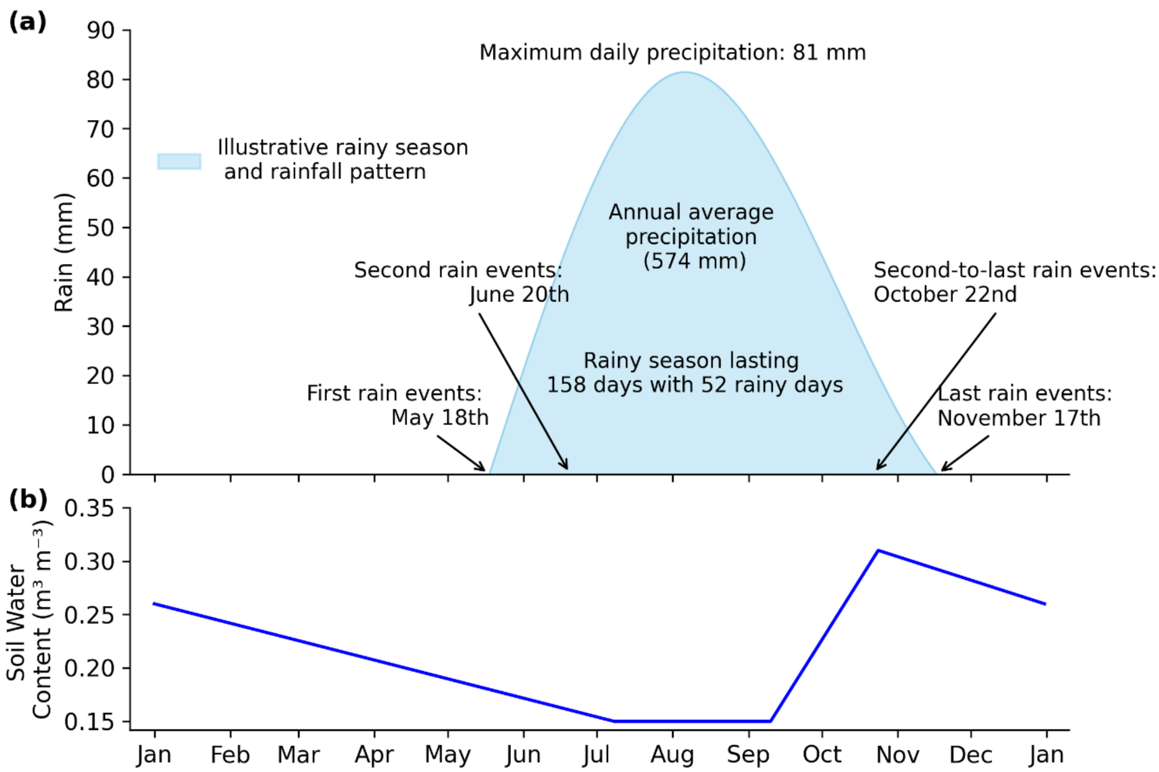

Figure S3: Characteristics of average (a) daily precipitation time series for 2018-2022 and (b) the soil water content in the capillary fringe of the groundwater (SWCC) time series collected for 2019-2021 used for the sensitivity analysis of water availability. All the variables were averaged between years.

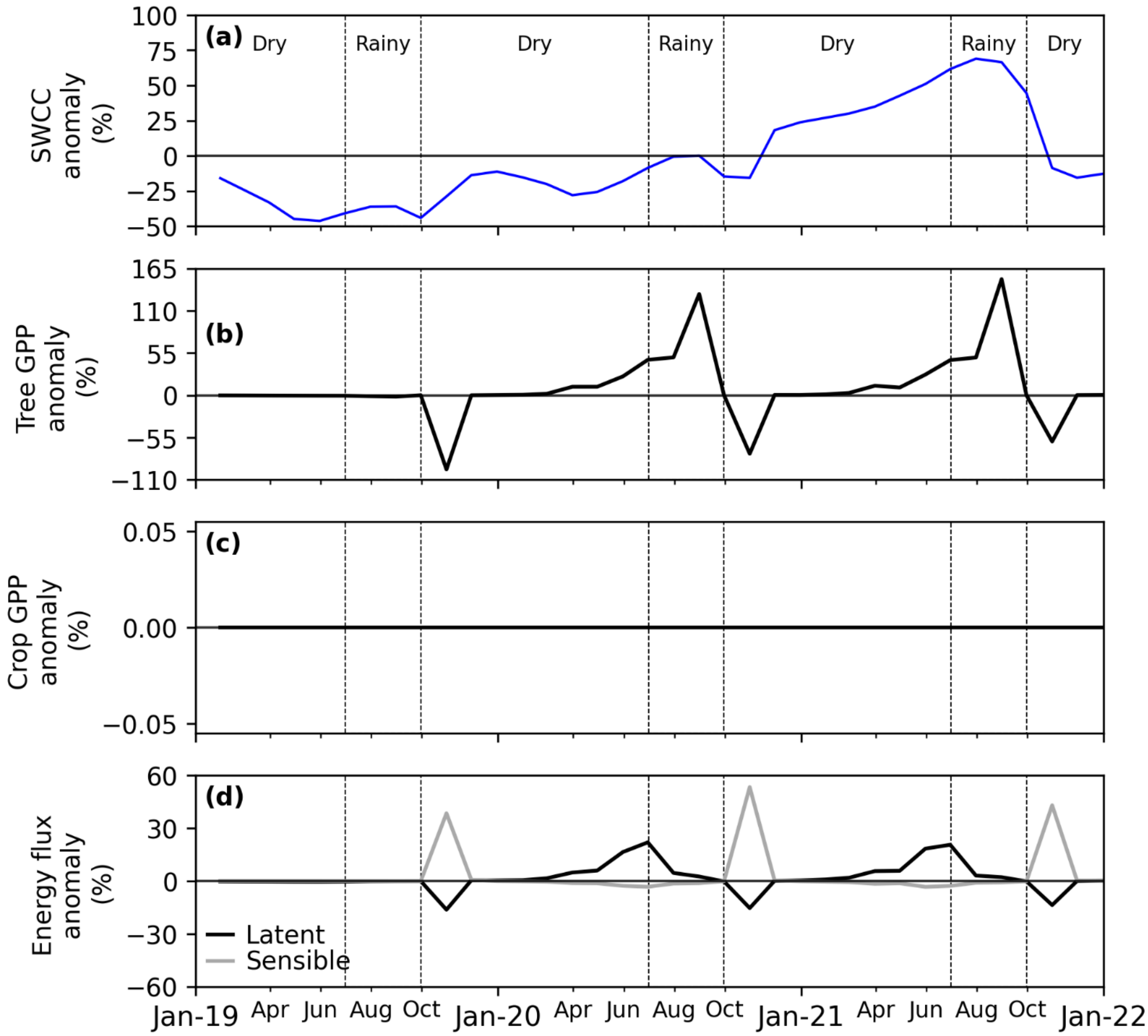

Figure S4: Sensitivity study of monthly anomalies in $R_{avg}SWCC_{var}$ scenario (a) soil water content in the capillary fringe of the groundwater table (SWCC), (b) tree gross primary productivity (GPP), (c) crop GPP, (d) latent and sensible flux. $R_{avg}SWCC_{var}$ is a simulation with average rain and variable SWCC, thus affecting the tree and the ecosystem, but not the crop. The sensitivity is quantified as the anomaly of the $R_{avg}SWCC_{var}$ scenario with respect to $R_{avg}SWCC_{avg}$ (simulation with average rain and average SWCC), considered as the reference scenario.

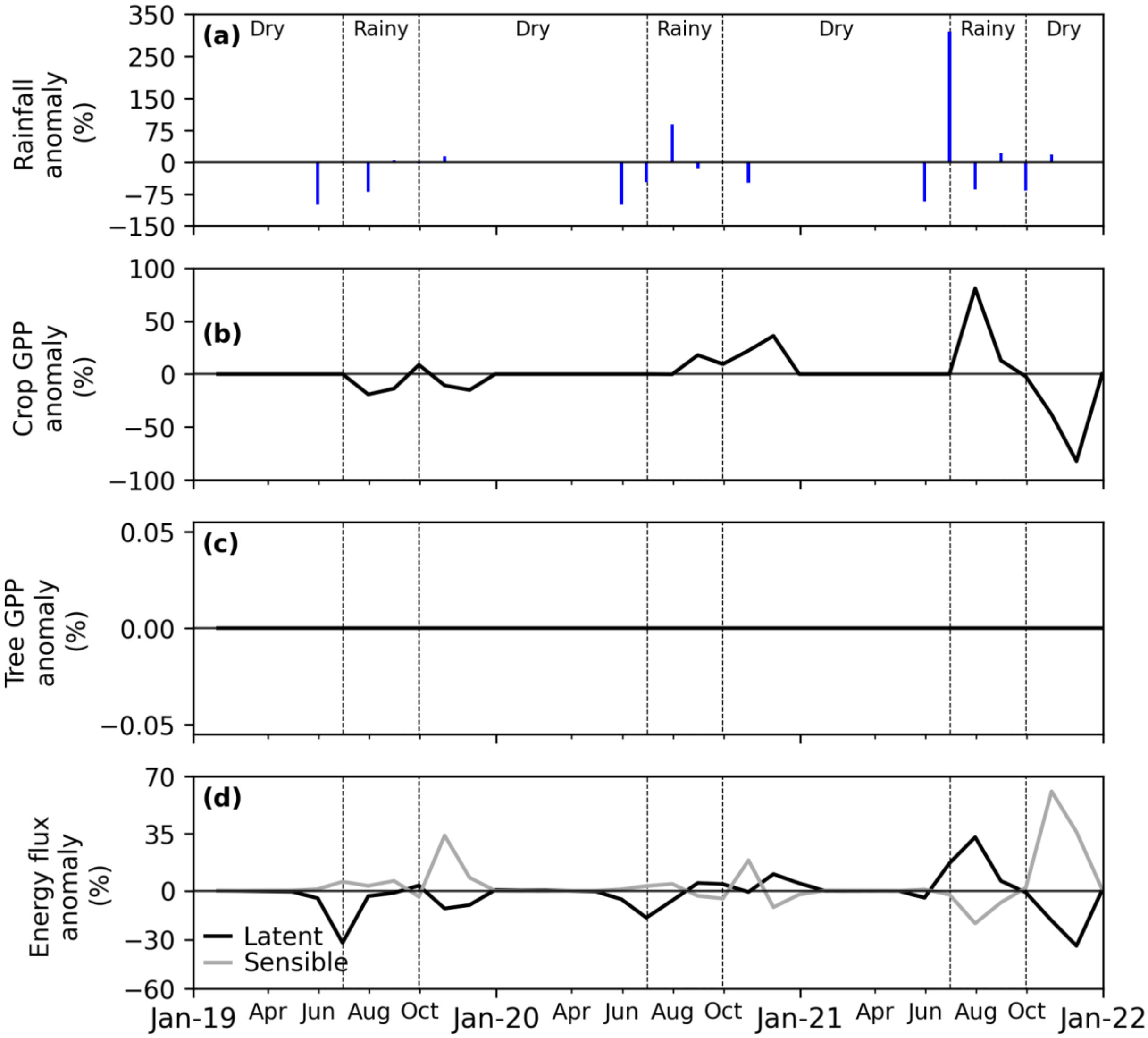

Figure S5: Monthly sensitivity study of anomalies in RvarSWCCavg scenario (a) rainfall, (b) crop gross primary productivity (GPP), (c) tree GPP, (d) latent and sensible flux. RvarSWCCavg is a simulation with variable rain and average SWCC, thus affecting the crop and the ecosystem, but not the tree. The sensitivity is quantified as the anomaly of the RvarSWCCavg scenario with respect to RavgSWCCavg (simulation with average rain and average SWCC), considered as the reference scenario.

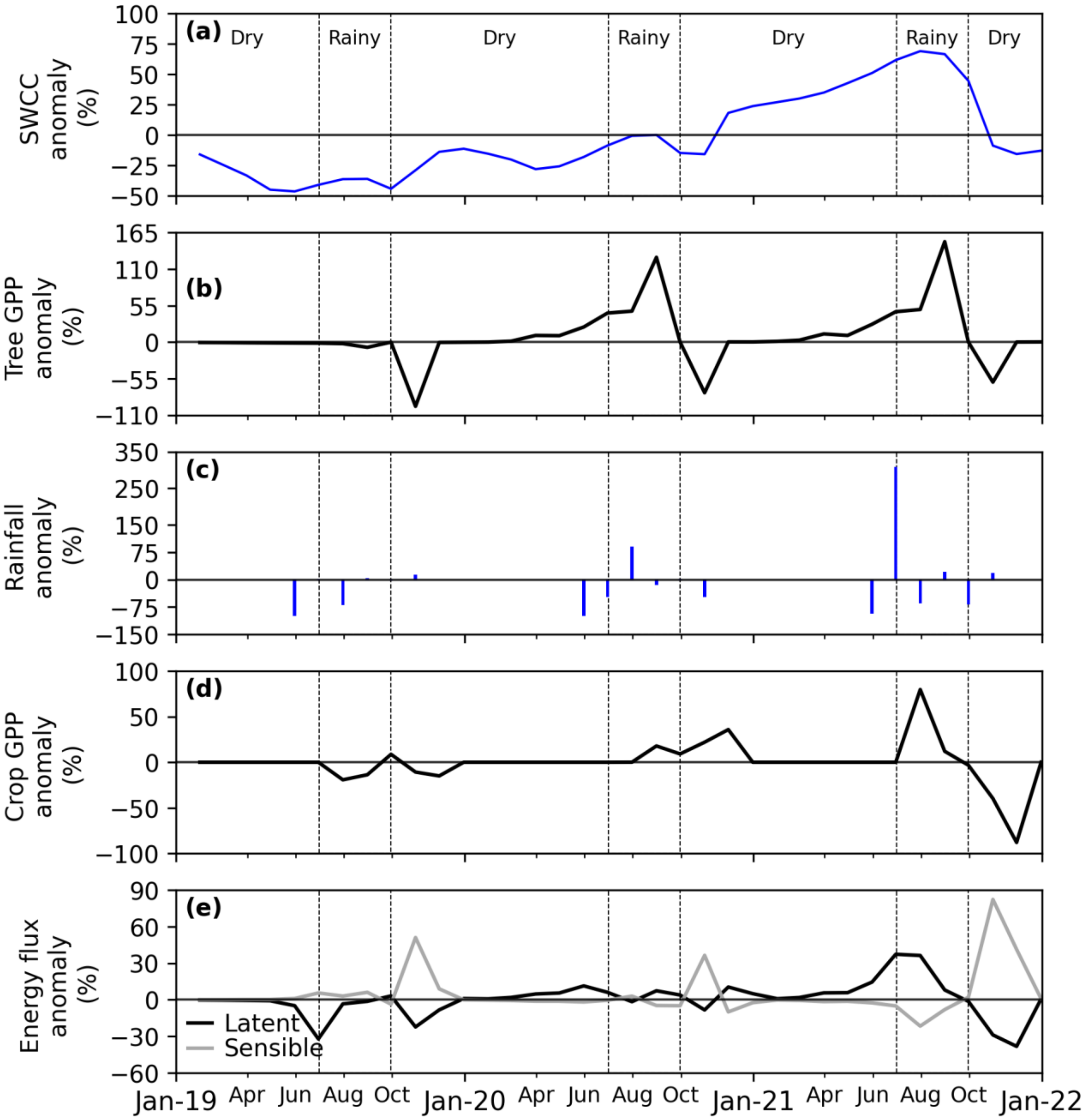

Figure S6: Monthly sensitivity study of anomalies in RvarSWCCvar scenario (a) soil water content in the capillary fringe of the groundwater table (SWCC), (b) tree gross primary productivity (GPP), (c) rainfall, (d) crop GPP, (e) latent and sensible flux. RvarSWCCvar is a simulation with variable rain and variable SWC, where crop, tree, and ecosystem are affected. The sensitivity is quantified as the anomaly of the RvarSWCCvar scenario with respect to RavgSWCCavg (simulation with average rain and average SWCC), considered as the reference scenario.

References

Bernacchi, C. J., Portis, A. R., Nakano, H., Caemmerer, S. von, and Long, S. P.: Temperature Response of Mesophyll Conductance. Implications for the Determination of Rubisco Enzyme Kinetics and for Limitations to Photosynthesis in Vivo, Plant Physiol., 130, 1992, https://doi.org/10.1104/pp.008250, 2002.

Chen, Q., Baldocchi, D., Gong, P., and Dawson, T.: Modeling radiation and photosynthesis of a heterogeneous savanna woodland landscape with a hierarchy of model complexities, Agric. For. Meteorol., 148, 1005–1020, https://doi.org/10.1016/j.agrformet.2008.01.020, 2008.

Diongue, D. M. L., Roupsard, O., Do, F. C., Stumpp, C., Orange, D., Sow, S., Jourdan, C., and Faye, S.: Evaluation of parameterisation approaches for estimating soil hydraulic parameters with HYDRUS-1D in the groundnut basin of Senegal, Hydrol. Sci. J., 67, 2327–2343, https://doi.org/10.1080/02626667.2022.2142474, 2022.

Diongue, D. M. L., Stumpp, C., Roupsard, O., Orange, D., Do, F. C., and Faye, S.: Estimating water fluxes in the critical zone using water stable isotope approaches in the Groundnut and Ferlo basins of Senegal, Hydrol. Process., 37, e14787, https://doi.org/10.1002/hyp.14787, 2023.

Harley, P. C., Thomas, R. B., Reynolds, J. F., and Strain, B. R.: Modelling photosynthesis of cotton grown in elevated CO2, Plant Cell Environ., 15, 271–282, https://doi.org/10.1111/j.1365-3040.1992.tb00974.x, 1992.

Kattge, J., Knorr, W., Raddatz, T., and Wirth, C.: Quantifying photosynthetic capacity and its relationship to leaf nitrogen content for global-scale terrestrial biosphere models, Glob. Change Biol., 15, 976–991, https://doi.org/10.1111/j.1365-2486.2008.01744.x, 2009.

Massad, R.-S., Tuzet, A., and Bethenod, O.: The effect of temperature on C4-type leaf photosynthesis parameters, Plant Cell Environ., 30, 1191–1204, https://doi.org/10.1111/j.1365-3040.2007.01691.x, 2007.

Roupsard, O., Audebert, A., Ndour, A. P., Clermont-Dauphin, C., Agbohessou, Y., Sanou, J., Koala, J., Faye, E., Sambakhe, D., Jourdan, C., le Maire, G., Tall, L., Sanogo, D., Seghieri, J., Cournac, L., and Leroux, L.: How far does the tree affect the crop in agroforestry? New spatial analysis methods in a Faidherbia parkland, Agric. Ecosyst. Environ., 296, https://doi.org/10.1016/j.agee.2020.106928, 2020.

Roupsard, O., Faye, W., Sow, S., Diongue, D. M. L., Orange, D., Do, F. C., Jourdan, C., Stumpp, C., and Faye, S.: Inverted phenology of #Faidherbia albida# paced with the dynamics of the water table, Congrès mondial d'agroforesterie, public, 5, 1 p., 2022.

Siegwart, L., Bertrand, I., Roupsard, O., and Jourdan, C.: Contribution of tree and crop roots to soil carbon stocks in a Sub-Sahelian agroforestry parkland in Senegal, Agric. Ecosyst. Environ., 352, 108524, https://doi.org/10.1016/j.agee.2023.108524, 2023.

Sow, S., Senghor, Y., Sadio, K., Vezy, R., Roupsard, O., Affholder, F., N'dienor, M., Clermont-Dauphin, C., Gaglo, E. K., Ba, S., Tounkara, A., Balde, A. B., Agbohessou, Y., Seghieri, J., Sall, S. N., Couedel, A., Leroux, L., Jourdan, C., Diaite, D. S., and Falconnier, G. N.: Calibrating the STICS soil-crop model to explore the impact of agroforestry parklands on millet growth, Field Crops Res., 306, 109206, https://doi.org/10.1016/j.fcr.2023.109206, 2024.

Thornley, J. H. M.: Instantaneous Canopy Photosynthesis: Analytical Expressions for Sun and Shade Leaves Based on Exponential Light Decay Down the Canopy and an Acclimated Non-rectangular Hyperbola for Leaf Photosynthesis, Ann. Bot., 89, 451–458, https://doi.org/10.1093/aob/mcf071, 2002.

Von Caemmerer, S.: Biochemical Models of Leaf Photosynthesis, Csiro Publishing, 186 pp., 2000.

Wickens, G. E.: Role of Acacia Species in the Rural Economy of Dry Africa and the Near East, Food & Agriculture Org., 144 pp., 1995.